CRYSTAL GROWTH & DESIGN

Article

pubs.acs.org/crystal

Two Anhydrous and a Trihydrate Form of Tilorone Dihydrochloride: Hydrogen-Bonding Patterns and Reversible Hydration/Dehydration Solid-State Transformation

Published as part of the Crystal Growth & Design virtual special issue In Honor of Prof. G. R. Desiraju

Vladimir V. Chernyshev,*[,†,‡] Alexandr V. Yatsenko,[†] Sergey V. Pirogov,[§] Tamara F. Nikulenkova,[§] Ekaterina V. Tumanova,[§] Ivan S. Lonin,[‡] Ksenia A. Paseshnichenko,[†] Andrei V. Mironov,[†] and Yurii A. Velikodny[†]

[†]Department of Chemistry, M. V. Lomonosov Moscow State University, 1-3 Leninskie Gory, Moscow 119991, Russian Federation

[‡]A. N. Frumkin Institute of Physical Chemistry and Electrochemistry RAS, 31 Leninsky Prospect, Moscow 119071, Russian Federation

[§]The Medical-Biological Research-Industrial Complex CYTOMED, 2 Muchnoy pereulok, St. Petersburg 191023, Russian Federation

Supporting Information

ABSTRACT: During the polymorph screening of an active pharmaceutical ingredient tilorone dihydrochloride (chemical name 2,7-bis[2-(diethylamino)ethoxy]-9-fluorenone dihydrochloride) two new polymorphic modifications — **III** and **IV** — were obtained. The crystal structures of both polymorphs were established from X-ray powder diffraction. An interesting phenomenon has been observed at ambient conditions for **III**, which transforms into a novel hydrated form **IIIh** during 2−3 h when the humidity in the storage room increases to 70% or more. As soon as the relative humidity falls to 30% or less, **IIIh** transforms into the parent anhydrous form **III** within an hour. Form **IIIh** has been identified as a trihydrate of tilorone dihydrochloride, and its crystal structure has been established from X-ray powder diffraction. On the basis of the crystal structures and hydrogen-bonding patterns, a mechanistic model of reversible hydration/dehydration solid-state transformation **III** ↔ **IIIh** depending on the relative humidity is proposed.

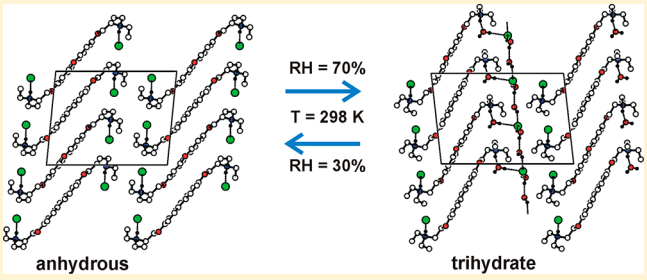

INTRODUCTION

Tilorone dihydrochloride (trade name Amixin IC), the orange water-soluble dihydrochloride salt of 2,7-bis[2-(diethylamino)-ethoxy]-9-fluorenone, is an orally active antiviral agent with a broad spectrum of action.[1−6] In 1996 tilorone was approved by Pharmacological Committee of Russian Federation for viral infection therapeutics and prophylaxis, and since 2005 it has been widely used in Ukraine.

Pharmaceutical solids can exist in multiple crystalline forms, and this phenomenon is known as polymorphism.[7−12] A recent study estimated that 80−90% organic compounds are able to exist in polymorphic forms.[13] Physicochemical properties of polymorphs, e.g., melting point, density, morphology, solubility and color, can differ significantly. In turn, this may have an impact on the stability, bioavailability and processability during manufacturing and/or at the stage of final product.[14] It should be noted that transformations between various crystalline forms (e.g., hydration, dehydration and polymorphic transformations) are often induced by environmental changes and may occur during drug manufacturing processes or during storage of a drug substance or dosage form.[15] The multitude and diversity

Scheme 1. Tilorone dihydrochloride

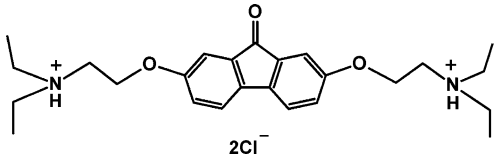

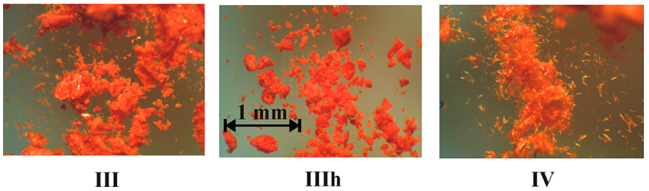

Figure 1. Microscopy photographs of the studied samples.

Received: August 28, 2012
Revised: October 24, 2012
Published: October 29, 2012

Table 1. Crystal Data for III, IIIh and IV

	III	IIIh	IV
empirical formula	$C_{25}H_{36}N_2O_3^{2+}\cdot 2Cl^-$	$C_{25}H_{36}N_2O_3^{2+}\cdot 2Cl^-\cdot 3H_2O$	$C_{25}H_{36}N_2O_3^{2+}\cdot 2Cl^-$
formula weight	483.46	537.51	483.46
particle morphology, color	no specific habit, orange	no specific habit, dark orange	needle, orange
wavelength, Å	1.54059	1.54059	1.78897
crystal system	monoclinic	monoclinic	monoclinic
space group	$P2_1/c$	$P2_1/c$	$P2_1/n$
a, Å	15.7674(18)	17.7102(19)	18.7680(17)
b, Å	13.3128(15)	13.3601(17)	19.6955(19)
c, Å	12.2800(14)	12.1598(16)	6.9450(11)
β, °	95.71(2)	96.39(2)	95.096(18)
volume, Å^3	2564.9(5)	2859.2(6)	2557.0(5)
M_{20}[a]	25	30	45
F_{30}[b]	51 (0.008, 62)	72 (0.006, 69)	117 (0.004, 58)
Z	4	4	4
D_x, g cm^{-3}	1.252	1.249	1.256
$2\theta_{min} - 2\theta_{max}$, increment, °	3.00 − 80.0, 0.01	3.00 − 80.0, 0.01	5.00 − 80.0, 0.01
no. params/restraints	172/110	184/102	172/110
$R_p/R_{wp}/R_{exp}$[c] [R_p/R_{wp}, Pawley fit]	0.028/0.036/0.020 [0.024/0.032]	0.025/0.032/0.022 [0.021/0.029]	0.024/0.032/0.022 [0.022/0.030]
goodness-of-fit	1.695	1.437	1.352

[a] M_{20} is defined according to ref 50. [b] F_{30} is defined according to ref 51. [c] R_p, R_{wp} and R_{exp} are defined according to ref 52.

of solid forms require a thorough understanding of solid-state phenomena that may occur in pharmaceutical materials. This can be achieved by applying various analytical methods.[16,17]

So far two polymorphic modifications of anhydrous tilorone dihydrochloride — monoclinic **I** (a = 8.32 Å, b = 43.32 Å, c = 7.08 Å, β = 93.9°) and orthorhombic **II** (a = 8.55 Å, b = 39.81 Å, c = 7.38 Å) — along with the characteristic powder patterns were reported.[18] In the framework of the polymorph screening carried out by our group, two new polymorphic modifications — **III** and **IV** — were obtained and characterized by various methods including DSC, TGA, IR and NMR spectroscopy, and X-ray powder diffraction. The powder patterns of **III** and **IV** were initially measured in February and successfully indexed in monoclinic unit cells with the volumes of 2565 and 2557 Å^3, respectively. Three months later (in May) new X-ray measurements of the same samples revealed that **IV** was stable, while **III** transformed into a new form (**IIIh**) with a new powder pattern indexed in the monoclinic unit cell with the volume of 2850 Å^3. All measurements were carried out at one diffractometer and at the same temperature 25 °C. The only difference was found outside the experimental room, and it was the difference in the outdoor temperature, which, however, resulted in different relative humidity in experimental room — around 30% in February and around 70% in May. That is why the hydration seems to be responsible for the solid-state transformation **III** → **IIIh**. The volume of the asymmetric part of **IIIh** is 75 Å^3 (Z = 4) larger than that of **III**, assuming that three or four water molecules per asymmetric unit could be absorbed. Visually, samples **III** and **IIIh** can be distinguished only by a slight color difference (**III** is orange and **IIIh** dark orange), while the morphology of both compounds is identical, because their crystallites have no specific habit (Figure 1). The particle morphology of **IV** is easily identified as needle.

The importance of hydration/dehydration processes in pharmaceuticals has been well-known for a long time,[19] because pharmaceutical solids as raw materials or as dosage forms often come in contact with water in the course of processing and storage. This may occur during crystallization, lyophilization, wet granulation, or spray drying, and because of exposure to humid air upon handling and storage. Hydrates often have unique spectra, diffraction patterns, or thermograms and thus can be easily distinguished from other hydrate species or anhydrous states using the respective methods, and many of these methods were used in recent investigations of hydration processes in pharmaceuticals.[17,20] For the crystalline pharmaceutical solids, the known crystal structures of anhydrous and hydrated forms offer valuable information, which helps to understand the specificity of hydration/dehydration processes and apply *ab initio* calculations in their quantifications. The most powerful technique used for crystal structure determination is single-crystal X-ray diffraction. However, it is often difficult to grow suitable-quality single crystals of biologically active organic compounds and therefore, pharmaceuticals: the growing procedure results only in polycrystalline powders. Even if single crystals of good quality are successfully grown, they may lose their integrity during hydration/dehydration transformations, producing a polycrystalline phase. Fortunately, there are methods for structure determination of organic molecular materials from powder X-ray diffraction data.[21−29] These methods were successfully applied in structural studies of polymorphic modifications and hydrated forms of various pharmaceuticals, such as acrinol,[30] finasteride[31] and sulfathiazole[32] among many others.

Inspired by the efficiency of powder diffraction methods in crystal structure determination, we have applied them to three aforementioned forms of tilorone dihydrochloride, namely, **III**, **IIIh** and **IV** (see Figure 1), in an attempt to find: (i) the reasons for different physicochemical properties of **III** and **IV**, and (ii) a model of reversible hydration/dehydration solid-state transformation **III** ↔ **IIIh** at ambient conditions. Herewith we present the results of our study.

EXPERIMENTAL SECTION

Materials. All initial reagents and solvents were commercially available and used as received. Tilorone base, i.e., 2,7-bis[2-(diethylamino)ethoxy]-9-fluorenone, was prepared following the known method.[3]

dx.doi.org/10.1021/cg3012475 | Cryst. Growth Des. 2012, 12, 6118−6125

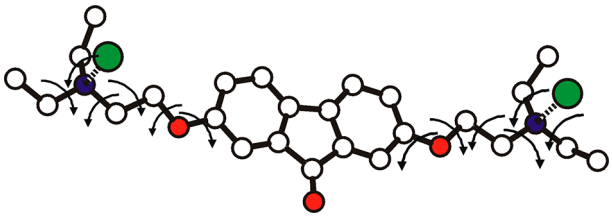

Figure 2. Model used in a search for structure solution. Torsion angles varied in simulated annealing runs are shown by arrows. The N···Cl distances (dashed lines) were fixed to 3.1 Å.

IR-Spectra and Elemental Analysis. IR absorption spectra of compounds **III** and **IV** were recorded in the wave range 3000−400 cm^{-1} with a resolution of 2 cm^{-1} using a Shimadzu FTIR-8400S spectrometer with KBr pellets. C, H and N analysis was carried out using a LECO CHNS-932 elemental analyzer.

Differential Scanning Calorimetry (DSC) and Thermogravimetric Analysis (TGA). Thermal studies were carried out using a Netzsch STA 449 F3 differential scanning calorimeter with Netzsch Proteus 5.2.1 software. The instrument was calibrated for temperature with pure benzophenone (mp 48.0 °C) and indium (mp 156.6 °C), and the energy calibration was performed with pure indium (purity 99.999%, heat of fusion 28.45 J g^{-1}). 10−15 mg of each sample was poured into a capped Al_2O_3 pan and heated to 280 °C with a ramp rate of 10 K min^{-1} under dry argon flow (protective purge 20 mL min^{-1}, sample purge 30 mL min^{-1}).

NMR Measurements. NMR spectra were measured at 305 K using a Bruker Advance III (600 MHz) spectrometer for D_2O solution. ^1H and ^{13}C NMR spectra were recorded with TMS as the external standard. The ^{15}N scale is given relative to 100% liquid NH_3 (δN = 0.0). All experiments were based on the Bruker standard techniques. $^1H-^{15}N$ gHMBC spectrum was recorded with 125 ms delay for evolution of long-range coupling.

Synthesis of III. Tilorone base (31.5 g, 0.077 mol) was mixed with 40 mL of acetone with stirring and then 13.7 mL of 35% HCl was added to pH 3−4 (Congo). The reaction mixture was incubated for 2 h at room temperature. The precipitate was filtered, washed with acetone, dried in air and then *in vacuo* to constant mass at 40−45 °C. A 32.95 (0.068 mol) mass of **III** was recovered as orange crystalline powder. Yield: 88%. Elemental analysis and IR data for **III** are presented in Supporting Information.

III can also be obtained from **IIIh** under ambient conditions when the relative humidity is decreased to 30% or less.

Synthesis of IIIh. Tilorone dihydrochloride (25.0 g, 0.0517 mol) was dissolved in 50 mL of water at 65−70 °C. Solution was filtered, and 300 mL of acetone was added to the filtrate. After being stirred for 15 min the mixture was cooled to −20 °C. The upper acetone layer was removed by decantation after 2 h. The lower layer containing the main part of tilorone dihydrochloride was exposed to air at room temperature to complete evaporation of solvent. The solid residue was triturated. A 22.0 g (0.041 mol) mass of **IIIh** was recovered as dark orange crystalline powder. Yield: 79%.

The DTA curve (see Figure S1 in Supporting Information) shows a 9.79% mass loss for **IIIh** on heating from ambient temperature to 205 °C, attributed to hydration water release. Such mass loss corresponds to 2.9 H_2O molecules per one formula unit of tilorone dihydrochloride. On the basis of these data and the difference in unit cell volume of **IIIh** and **III**, it was proposed that the **IIIh** form is a trihydrate. This conclusion agrees with the elemental analysis data presented in Supporting Information.

IIIh can also be obtained from **III** under ambient conditions when the relative humidity is increased to 70% or more.

Synthesis of IV. Tilorone base (31.0 g, 0.076 mol) was mixed with 100 mL of dry *iso*-propanol with stirring and then 13.4 mL of 35% HCl were added to pH 3−4 (Congo). The reaction mixture was heated to 70−75 °C, cooled to room temperature (a seed can be used) and then to 7−10 °C. After incubation for 4 h the precipitate was filtered, washed with cold dry isopropanol, dried in air and then *in vacuo* to constant mass at 40−45 °C. A 28.25 g (0.058 mol) mass of **IV** was recovered as orange crystalline powder. Yield: 76%. Elemental analysis, IR and NMR data for **IV** are presented in Supporting Information.

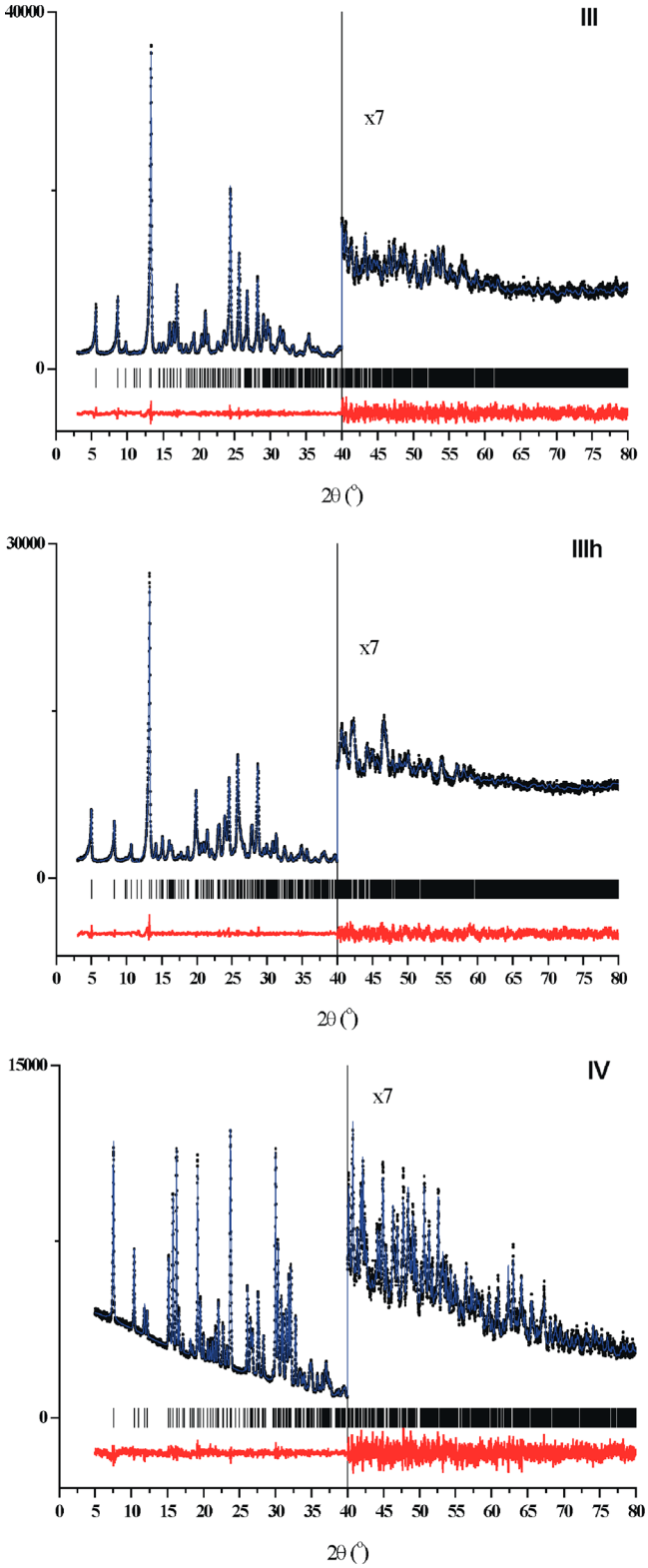

Figure 3. The Rietveld plots for **III** (top), **IIIh** (middle), and **IV** (bottom) showing the experimental (black dots), calculated (blue) and difference (red) curves. The vertical bars denote calculated positions of the diffraction peaks.

dx.doi.org/10.1021/cg3012475 | *Cryst. Growth Des.* 2012, 12, 6118−6125

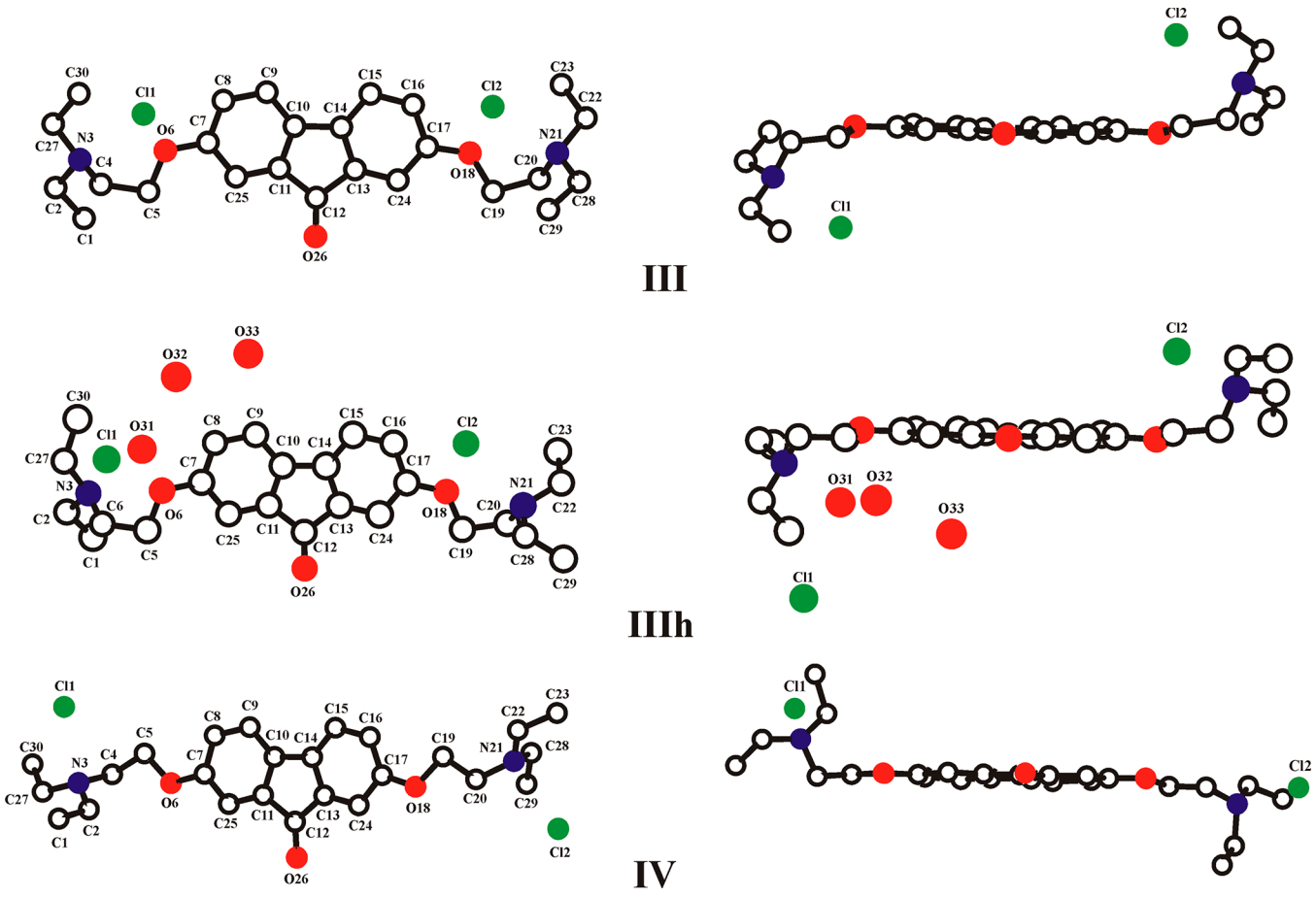

Figure 4. Asymmetric part of **III** (top), **IIIh** (middle) and **IV** (bottom) viewed in two approximately orthogonal projections. Displacement spheres are drawn at the 50% probability level; H atoms are omitted for clarity.

Powder X-ray Diffraction. Powder patterns were measured using three powder diffractometers, namely, Huber G670 Guinier camera (Cu Kα_1 radiation, λ = 1.54059 Å, transmission mode), Stoe STADI-P (CoK$_{\alpha 1}$ radiation, λ = 1.788965 Å, transmission mode) and EMPYREAN (Cu Kα radiation, Ni β-filter, Bragg–Brentano mode). The latter diffractometer equipped with a vacuum camera has been used for quick data collection *in vacuo*. The powder patterns for structure solution and subsequent refinement were collected at Huber G670 (for **III** and **IIIh**) and Stoe STADI-P (for **IV**); see Table 1 for data collection details.

Structure Determination. For all compounds, the monoclinic cell dimensions were determined using three indexing programs: TREOR90,[33] ITO,[34] and AUTOX.[35,36] On the basis of systematic extinctions, the space group for **III** and **IIIh** was determined to be $P2_1/c$, and for **IV** – $P2_1/n$. The unit-cell parameters and space groups were further tested using a Pawley fit[37] and confirmed by crystal structure solution. The crystal data, data collection and refinement parameters for three compounds are given in Table 1. The crystal structures have been solved with the use of a simulated annealing technique.[38] The Cambridge Structural Database (CSD, Version 5.33)[39] contains no structures with the 2,7-bis[2-(diethylamino)-ethoxy]-9-fluorenone fragment. Therefore, the initial molecular model of tilorone dihydrochloride (Figure 1) has been obtained in the course of density functional theory (DFT) calculations *in vacuo* using the quantum-chemical code Priroda[40−43] employing the generalized-gradient approximation (GGA) and PBE exchange correlation functional.[44] During the subsequent direct space search for structure solution, the tetrahedral environment of N atoms in the obtained molecular model was considered as a rigid unit with the N···Cl distance fixed to 3.1 Å; H atoms were omitted. In the simulated annealing runs, the total number of varied degrees of freedom (DOF) for **III** and **IV** was 18 — 3 translational, 3 orientational and 12 torsional, shown by arrows in Figure 2.

The use of initial model with three separate fragments — one cation and two anions, and six more DOFs gave the same solutions for **III** and **IV**. Nine more DOFs were used in a solution search for **IIIh**, where each water oxygen required three translational parameters. The solution found was fitted with the program MRIA[45] in the bond-restrained Rietveld refinement using a split-type pseudo-Voigt peak profile function.[46] A comparison of powder patterns measured in transmission and reflection modes for all compounds showed weak texture effects in the patterns of **III** and **IIIh** with [001] as a direction of preferred orientation, and moderate texture in **IV**, where the crystallites are needle-shaped (Figure 1). Therefore, two formalisms of preferred orientation correction — March-Dollase[47] (for **III** and **IIIh**) and spherical harmonics expansion up to the sixth order[48,49] (for **IV**) — were used in the refinement. Restraints were applied to the intramolecular bond lengths and contacts (<2.8 Å); the strength of the restraints was a function of interatomic separation and, for intramolecular bond lengths, corresponded to r.m.s. deviation 0.02 Å. Additional restraints were applied to the planarity of ring systems with the attached atoms, with the maximal allowed deviation from the mean plane of 0.03 Å. All non-H atoms were refined isotropically. During the refinement of **IIIh**, the isotropic displacement parameter U_{iso} of Cl1 reached a high value of 0.3 Å^{-2} and more, while U_{iso} of one water oxygen (O31) was negative, indicating that sorts of these two atoms have to be permutated. After such permutation, the U_{iso} parameters of Cl1 and O31 in new positions were refined to normal values with the decreased values of profile R-factors. In all structures, H atoms were positioned geometrically (C–H 0.93–0.97 Å; N–H 0.91 Å; O–H 0.85 Å) and not refined. For all compounds, the

dx.doi.org/10.1021/cg3012475 | *Cryst. Growth Des.* 2012, 12, 6118–6125

diffraction profiles after the final bond-restrained Rietveld refinements are shown in Figure 3 and molecular structures — in Figure 4.

RESULTS AND DISCUSSION

For all compounds, the crystal packing exhibits multiple hydrogen bonds, both strong and weak,[53] which are summarized in Table 2.

Table 2. Hydrogen-Bonding Geometry (Å, °) in III, IIIh, and IV[a]

	D−H···A	D−H	H···A	D···A	D−H···A
III					
	N3−H3···Cl1	0.91	2.11	3.011(10)	169
	N21−H21···Cl2	0.91	2.12	3.021(9)	172
	C22−H22A···Cl2^{i}	0.97	2.66	3.521(11)	148
	C23−H23A···O26^{ii}	0.96	2.50	3.438(13)	164
	C27−H27A···Cl1^{iii}	0.97	2.59	3.483(12)	152
	C29−H29B···O26^{iv}	0.96	2.53	3.358(13)	144
IIIh					
	N21−H21···O31	0.91	2.11	3.021(13)	175
	N3−H3···Cl1	0.91	1.89	2.759(16)	159
	O31−H31A···Cl1	0.85	2.50	3.343(12)	172
	O32−H32A···Cl1^{v}	0.85	2.47	3.263(11)	156
	O32−H32B···O31	0.85	1.87	2.712(15)	171
	O33−H33A···Cl1^{vi}	0.85	2.41	3.150(11)	146
	O33−H33B···O32	0.85	1.99	2.828(15)	167
	C28−H28B···O26^{vii}	0.97	2.50	3.420(19)	159
	C15−H15···Cl2^{viii}	0.93	2.57	3.480(16)	167
	C4−H4B···O33^{i}	0.97	2.50	3.334(19)	144
	C30−H30C···O32^{v}	0.96	2.48	3.40(2)	160
	C22−H22B···Cl2^{iii}	0.97	2.76	3.568(15)	141
IV					
	N3−H3···Cl1	0.91	2.13	3.043(6)	178
	N21−H21···Cl2	0.91	2.12	3.028(6)	173
	C4−H4B···O26^{ix}	0.97	2.40	3.305(10)	155
	C19−H19B···Cl1^{x}	0.97	2.79	3.511(8)	132
	C9−H9···Cl2^{xi}	0.93	2.77	3.613(8)	152

[a]Symmetry codes: (i) x, $3/2 - y$, $1/2 + z$; (ii) $-x$, $1/2 + y$, $3/2 - z$; (iii) x, $3/2 - y$, $z - 1/2$; (iv) $-x$, $1 - y$, $1 - z$; (v) $1 - x$, $2 - y$, $1 - z$; (vi) $1 - x$, $1/2 + y$, $1/2 - z$; (vii) $-x$, $1 - y$, $-z$; (viii) $-x$, $2 - y$, $1 - z$; (ix) $2 - x$, $-y$, $2 - z$; (x) $x - 1/2$, $1/2 - y$; $z - 3/2$; (xi) $3/2 - x$, $1/2 + y$, $-3/2 - z$.

The crystal structures of **III** and **IIIh** are closely related to each other. In both of them, cations and anions form layers parallel to (101) (Figure 5). In **III**, there are only two short contacts between these layers: O26···H23A and O26···H29B, both involving methyl H atoms (Table 2). In **IIIh**, the layers are joined by O−H···O hydrogen bonds between water molecules.

The layers in **III** and **IIIh** are presented in Figure 6. In both structures, the cations form stacks along the *c* axis direction. Within the stack, only the utmost benzene rings of adjacent cations overlap with centroid−centroid separations of 3.70(1) Å both in **III** and **IIIh**.

In **III**, chloride anions are located at the sides of stacks between diethylammonium groups, and each Cl^- forms a hydrogen bond Cl···H−N with one of these groups (Table 2). The layers in **III** are superimposed so that the stacks of cations in adjacent layers are slightly displaced relative to each other along the *a* axis direction (Figure 7, top). As a result, chloride anions have different environments: half of them (Cl1) are located in the channels along the *b* axis direction, whereas the rest (Cl2) are held between the cationic stacks of the lower and upper layers.

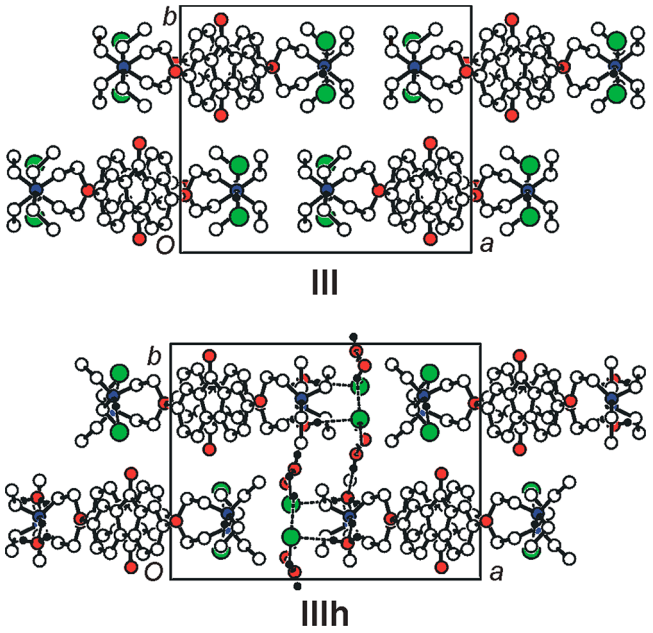

Figure 5. The layers in **III** (top) and **IIIh** (bottom) viewed along the *c* axis direction. Dashed lines denote strong hydrogen bonds. The C-bound H atoms are omitted for clarity.

Because of the nonequivalence of anionic positions illustrated in Figure 8, Cl1 forms only one Cl···H−C contact shorter than the sum of van der Waals radii (Cl1···H27A), whereas Cl2 has five short contacts.

In structure **IIIh**, the Cl2 anion retains a position inside the stack, whereas the Cl1 anion is displaced to the interstack space by one of water molecules, although is still within the layer (Figure 6, bottom). This is not an unexpected result: statistical analysis of the structures of hydrates of hydrochloric salts of aliphatic *tert*-amines containing two or more water molecules per each chloride anion (CSD, Version 5.33)[21] demonstrates that hydrogen bonds N−H···Cl and N−H···O are formed with approximately equal probability — 58 examples of the first type (N−H···Cl) against 50 examples of the second type (N−H···O). In **IIIh**, one water molecule (O31) forms two hydrogen bonds: one bond O···H−N with the diethylammonium group, and the other of the O−H···Cl type — with the Cl1 anion (Figure 6, bottom). Two remaining water molecules (O32 and O33) are joined by hydrogen bonds with Cl1 (Table 2) forming the nets parallel to (011) (Figure 9). These nets separate the neighboring stacks of cations; thus the stacks within each layer are pushed apart, as presented in Figure 7 (bottom). As a result, parameter *a* in **IIIh** becomes 1.94 Å longer than in **III**, whereas changes in *b* and *c* parameters are small.

In **IV**, the conformation of $(CH_2)_2NH^+(C_2H_5)_2$ side groups in the cation is distinct from that in **III** and **IIIh** (Figure 4). Packing of cations and anions in **IV** (Figure 10) also differs from those observed in **III** and **IIIh**. In **IV**, cations related by the *c* translation form stacks. Two adjacent stacks give a pillar, and chloride anions are located between the pillars. Each anion forms hydrogen bond with one diethylammonium group (Table 2). There are no layers in **IV**.

dx.doi.org/10.1021/cg3012475 | *Cryst. Growth Des.* 2012, 12, 6118−6125

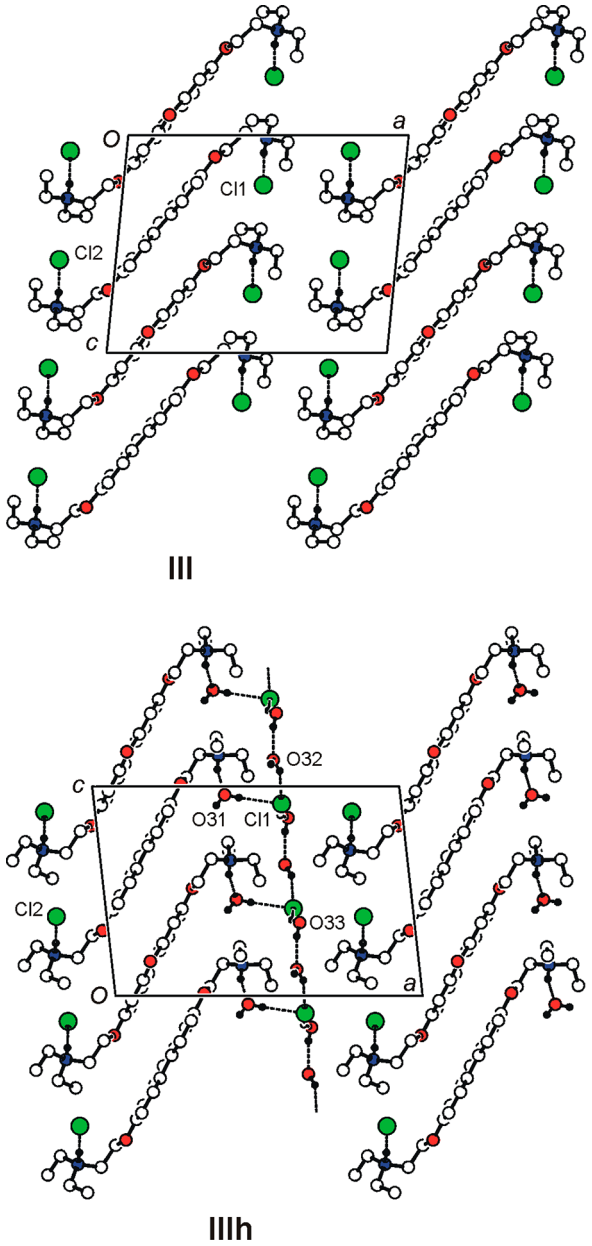

Figure 6. The layers in **III** (top) and **IIIh** (bottom) viewed along the *b* axis direction and showing cationic stacks. Dashed lines denote strong hydrogen bonds. The C-bound H atoms are omitted for clarity.

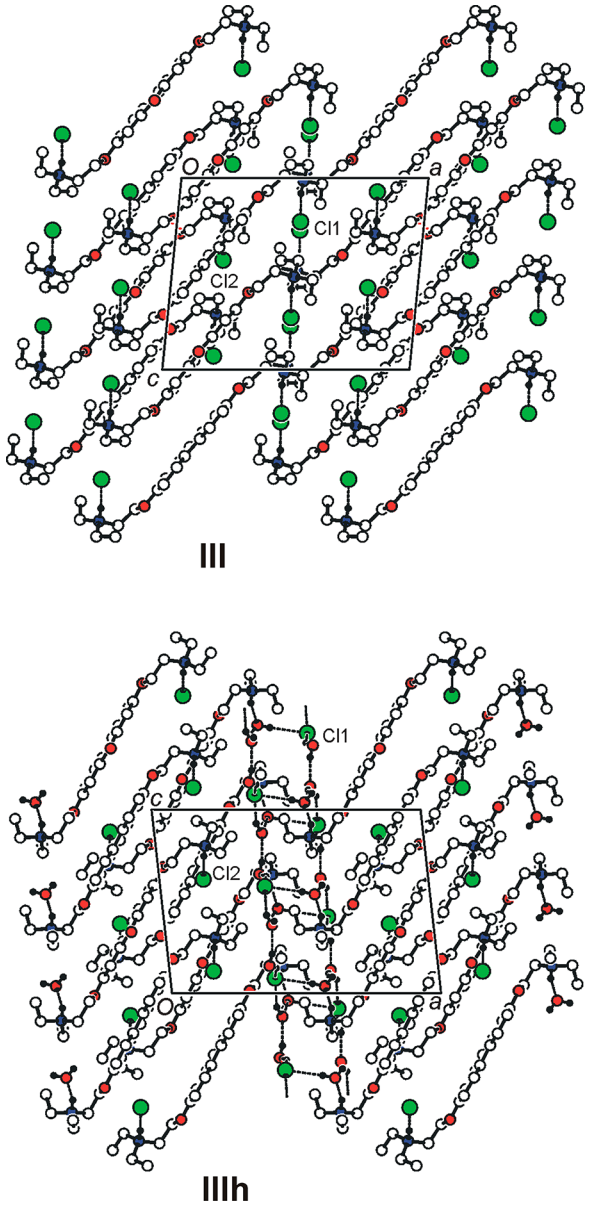

Figure 7. The crystal packing of **III** (top) and **IIIh** (bottom) viewed along the *b* axis direction and showing the overlapping of layers and nonequivalence of chloride anions. Dashed lines denote strong hydrogen bonds. The C-bound H atoms are omitted for clarity.

Structural data offer an explanation of easy reversible hydration of **III**: water molecules can penetrate into a crystal *via* interlayer boundaries and then enter the layers without disruption of the cation packing motif. In the same way, the absorbed water molecules can easily leave the crystals of **IIIh** keeping the cation packing motif without disturbance. Ease of dehydration of **IIIh** is supported by fast **IIIh** → **III** transformation *in vacuo*. Two powder patterns of **IIIh** were quickly (3 min each) measured using a diffractometer equipped with a vacuum pump. One pattern was measured at ambient conditions (red curve in Figure 11), and another one *in vacuo* (blue curve in Figure 11).

One can see that full solid-state transformation **IIIh** (red) → **III** (blue) *in vacuo* occurred within 1 min (or even faster). As follows from Figure 11, powder diffraction is a quick and reliable method for estimation of the phase content of a sample

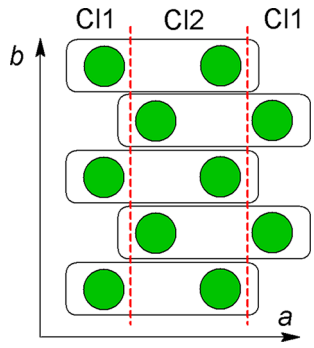

Figure 8. Schematic illustration of the nonequivalence of chloride anions in **III**. Anions Cl2 are held between the cationic stacks represented by rectangles.

dx.doi.org/10.1021/cg3012475 | *Cryst. Growth Des.* 2012, 12, 6118–6125

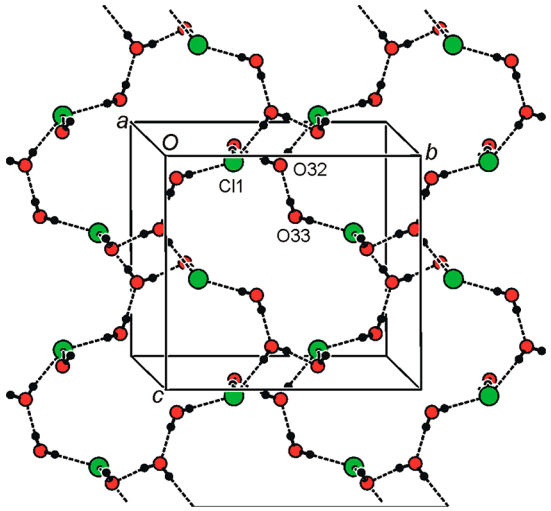

Figure 9. Hydrogen-bonding net in **IIIh** formed by anions and crystalline water molecules.

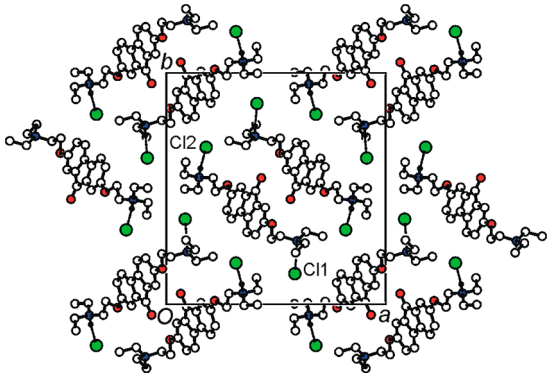

Figure 10. The crystal packing of **IV** viewed along the *c* axis direction. Dashed lines denote N---H···Cl hydrogen bonds. The C-bound H atoms are omitted for clarity.

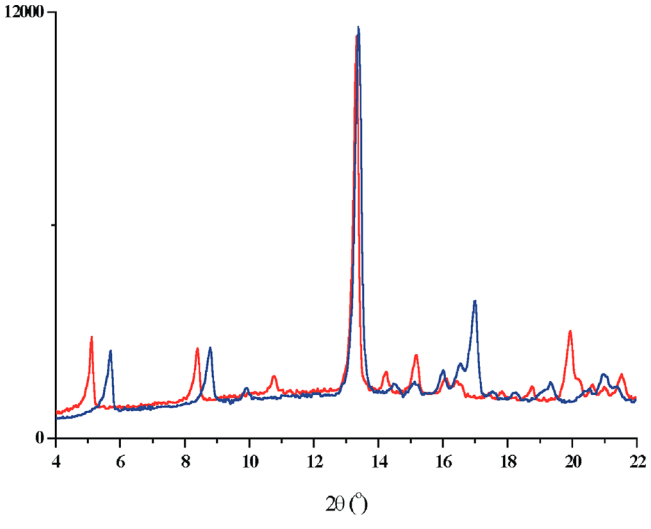

Figure 11. Two patterns of **IIIh** measured on EMPYREAN at T = 25 °C: red −3 min measurement at ambient conditions, P = 1 Kbar; blue −3 min measurement started 1 min after the vacuum pump was switched on, $P = 10^{-6}$ mbar.

of **III** during the storage. In **IV**, the ways suitable for penetration of water molecules into a crystal are absent; that is why hydration of this polymorph should be accompanied by complete rearrangement of crystal structure.

This study allowed us to clarify some aspects of reversible **III** ↔ **IIIh** transformation. However, several questions still remain unsolved. For example, in powder patterns measured for **III** and **IIIh** at various conditions we observed no additional peaks; all peaks were attributed either to **III** or to **IIIh**. Why were the hydrated crystalline forms of tilorone dihydrochloride with low water content — mono- or dihydrate — not observed? Another question concerns the minimum at 226.3 °C on the DSC curve for **IV** (Figure S1, top) — whether it corresponds to the phase transition or not. We hope to find answers to these new questions in the future.

CONCLUSIONS

In summary, three new forms of tilorone dihydrochloride — two anhydrous forms, **III** and **IV**, and a trihydrate form **IIIh** — were obtained, and their crystal structures were established from X-ray powder diffraction. Different crystal packings and hydrogen-bonding patterns of **III** and **IV** elucidate why one form is unstable to hydration at ambient conditions, while another is stable. In **III**, there are separate layers of hydrogen-bonded cations and anions, and atmospheric water can easily penetrate into a crystal *via* interlayer boundaries thus leading to solid-state formation of **IIIh**. The solid-state hydration/dehydration transformation **III** ↔ **IIIh** is reversible at ambient conditions and depends on the relative humidity only. In **IV**, there are no layers and thus no ways suitable for penetration of water molecules into a crystal, so hydration of this polymorph requires a complete rearrangement of crystal structure; that is why **IV** is much more stable than **III** during the long-term storage.

ASSOCIATED CONTENT

Supporting Information

Crystallographic information (.cif files), elemental analysis and IR data, experimental and calculated powder patterns for all compounds and NMR spectrum for **IV**. This material is available free of charge via the Internet at http://pubs.acs.org.

AUTHOR INFORMATION

Corresponding Author

*E-mail: vladimir@struct.chem.msu.ru. Tel.: +7-8-(495) 9393654. Fax: +7-8-(495)9390898.

Author Contributions

The manuscript was written through contributions of all authors. All authors have given approval to the final version of the manuscript.

Notes

The authors declare no competing financial interest.

ACKNOWLEDGMENTS

DSC and TGA studies were carried out in the X-ray diffraction Centre of St. Petersburg State University.

REFERENCES

(1) Krueger, R. F.; Mayer, G. D. *Science* **1970**, *169*, 1213−1214.
(2) Mayer, G. D.; Krueger, R. F. *Science* **1970**, *169*, 1214−1215.
(3) Andrews, E. R.; Fleming, R. W.; Grisar, J. M.; Kihm, J. C.; Wenstrup, D. L.; Mayer, G. D. *J. Med. Chem.* **1974**, *17*, 882−886.
(4) Chandra, P.; Wright, G. J. *Top. Curr. Chem.* **1977**, *72*, 125−148.

(5) Stringfellow, D. A.; Glasgow, L. A. *Antimicrob. Agents Chemother.* **1972**, *2*, 73−78.
(6) Fleming, R. W.; Wenstrup, D. L.; Andrews, E. R. U.S. Patent 3592819, 1971.
(7) Dunitz, J. D. *Pure Appl. Chem.* **1991**, *63*, 177−185.
(8) Bernstein, J. *Polymorphism in Molecular Crystals*; Oxford University Press: Oxford, 2002.
(9) Rodriguez-Spong, B.; Price, C. P.; Jayasankar, A.; Matzger, A. J.; Rodriguez-Hornedo, N. *Adv. Drug Delivery Rev.* **2004**, *56*, 241−274.
(10) Hilfiker, R. *Polymorphism in the Pharmaceutical Industry*; Wiley-VCH Verlag GmbH & Co. KGaA: Weinheim, 2006.
(11) Desiraju, G. R. *Cryst. Growth Des.* **2008**, *8*, 3−5.
(12) Brittain, H. G. *Polymorphism in Pharmaceutical Solids*, 2nd ed.; Informa Healthcare: New York, 2009; Vol. *192*.
(13) Stahly, G. *Cryst. Growth Des.* **2007**, *7*, 1007−1026.
(14) Byrn, S. R.; Pfeiffer, R. R.; Stowell, J. G. *Solid-State Chemistry of Drugs*, 2nd ed.; SSCI Inc.: West Lafayette, IN, 1999.
(15) Morris, K. R.; Griesser, U. J.; Eckhardt, C. J.; Stowell, J. G. *Adv. Drug Delivery Rev.* **2001**, *48*, 91−114.
(16) Stephenson, G. A.; Forbes, R. A.; Reutzel-Edens, S. M. *Adv. Drug Delivery Rev.* **2001**, *48*, 67−90.
(17) Chieng, N.; Rades, T.; Aaltonen, J. *J. Pharm. Biomed. Anal.* **2011**, *55*, 618−644.
(18) Ignatenko, O. A.; Kontsevoi, I. A.; Gabitov, A. F.; Pirogov, S. V. Patent application RU 2011152830 (15.12.2011).
(19) Byrn, S. R. *Solid-State Chemistry of Drugs*; Academic Press: New York, 1982.
(20) Brittain, H. G. *J. Pharm. Sci.* **2012**, *101*, 464−484.
(21) Harris, K. D. M.; Tremayne, M.; Lightfoot, P.; Bruce, P. G. *J. Am. Chem. Soc.* **1994**, *116*, 3543−3547.
(22) Harris, K. D. M.; Tremayne, M.; Kariuki, B. M. *Angew. Chem., Int. Ed.* **2001**, *40*, 1626−1651.
(23) Chernyshev, V. V. *Russ. Chem. Bull.* **2001**, *50*, 2273−2291.
(24) David, W. I. F.; Shankland, K.; McCusker, L. B.; Baerlocher, C., Eds. *Structure Determination from Powder Diffraction Data*, OUP/IUCr, 2002.
(25) Cheung, E. Y.; Kitchin, S. J.; Harris, K. D. M.; Imai, Y.; Tajima, N.; Kuroda, R. *J. Am. Chem. Soc.* **2003**, *125*, 14658−14659.
(26) Tremayne, M. *Phil. Trans. R. Soc.* **2004**, *362*, 2691−2707.
(27) Favre-Nicolin, V.; Cerny, R. *Z. Kristallogr.* **2004**, *219*, 847−856.
(28) Tsue, H.; Horiguchi, M.; Tamura, R.; Fujii, K.; Uekusa, H. *J. Synth. Org. Chem. Jpn.* **2007**, *65*, 1203−1212.
(29) David, W. I. F.; Shankland, K. *Acta Crystallogr., Sect. A* **2008**, *64*, 52−64.
(30) Fujii, K.; Uekusa, H.; Itoda, N.; Hasegawa, G.; Yonemochi, E.; Terada, K.; Pan, Z.; Harris, K. D. M. *J. Phys. Chem. C* **2010**, *114*, 580−586.
(31) Byard, S.; Abraham, A.; Boulton, P. J. T.; Harris, R. K.; Hodgkinson, P. *J. Pharm. Sci.* **2012**, *101*, 176−186.
(32) Munroe, A.; Rasmuson, A. C.; Hodnett, B. K.; Croker, M. D. *Cryst. Growth Des.* **2012**, *12*, 2825−2835.
(33) Werner, P.-E.; Eriksson, L.; Westdahl, M. *J. Appl. Crystallogr.* **1985**, *18*, 367−370.
(34) Visser, J. W. *J. Appl. Crystallogr.* **1969**, *2*, 89−95.
(35) Zlokazov, V. B. *J. Appl. Crystallogr.* **1992**, *25*, 69−72.
(36) Zlokazov, V. B. *Comput. Phys. Commun.* **1995**, *85*, 415−422.
(37) Pawley, G. S. *J. Appl. Crystallogr.* **1981**, *14*, 357−361.
(38) Zhukov, S. G.; Chernyshev, V. V.; Babaev, E. V.; Sonneveld, E. J.; Schenk, H. *Z. Kristallogr.* **2001**, *216*, 5−9.
(39) Allen, F. H. *Acta Crystallogr., Sect. B* **2002**, *B58*, 380−388.
(40) Laikov, D. N. *Chem. Phys. Lett.* **1997**, *281*, 151−154.
(41) Laikov, D. N. *Priroda Code*, version 5; Moscow State University: Moscow, 2004.
(42) Laikov, D. N.; Ustynyuk, Y. A. *Izv. Akad. Nauk, Ser. Khim.* **2005**, 804−810; (In Russian) *Russ. Chem. Bull.* **2005**, *54*, 820−826.
(43) Laikov, D. N. *Chem. Phys. Lett.* **2005**, *416*, 116−120.
(44) Perdew, J. P.; S. Burke, S.; Ernzerhof, M. *Phys. Rev. Lett.* **1996**, *77*, 3865−3868.
(45) Zlokazov, V. B.; Chernyshev, V. V. *J. Appl. Crystallogr.* **1992**, *25*, 447−451.
(46) Toraya, H. *J. Appl. Crystallogr.* **1986**, *19*, 440−447.
(47) Dollase, W. A. *J. Appl. Crystallogr.* **1986**, *19*, 267−272.
(48) Ahtee, M.; Nurmela, M.; Suortti, P.; Järvinen, M. *J. Appl. Crystallogr.* **1989**, *22*, 261−268.
(49) Järvinen, M. *J. Appl. Crystallogr.* **1993**, *26*, 525−531.
(50) de Wolff, P. M. *J. Appl. Crystallogr.* **1968**, *1*, 108−113.
(51) Smith, G. S.; Snyder, R. L. *J. Appl. Crystallogr.* **1979**, *12*, 60−65.
(52) Young, R. A.; Wiles, D. B. *J. Appl. Crystallogr.* **1982**, *15*, 430−438.
(53) Desiraju, G. R.; Steiner, T. *The Weak Hydrogen Bond in Structural Chemistry and Biology*; Oxford University Press: Oxford, 1999.